Proteomic Analysis of Tumor Establishment and Growth in the B16-F10 Mouse Melanoma Model

ARTICLE *in* JOURNAL OF PROTEOME RESEARCH · JUNE 2006

Impact Factor: 4.25 · DOI: 10.1021/pr060059q · Source: PubMed

6 AUTHORS, INCLUDING:

Rachel E Neal
University of Louisville
31 PUBLICATIONS **704** CITATIONS
SEE PROFILE

Donita Garland
Harvard University
65 PUBLICATIONS **5,044** CITATIONS
SEE PROFILE

research articles Journal of proteome research

Proteomic Analysis of Tumor Establishment and Growth in the B16-F10 Mouse Melanoma Model

W. David Culp,[*,†,§] Rachel Neal,[†] Robert Massey,[‡,§] Lars Egevad,[§] Pavel Pisa,[§] and Donita Garland[†]

Protein Biochemistry Section, National Eye Institute, National Institutes of Health, Bethesda, Maryland 20892, Tumor Research Institute, Washington, DC, and Department of Oncology and Pathology, Cancer Center Karolinska, Karolinska Hospital/Institute, 171 76 Stockholm, Sweden

Received February 22, 2006

The B16-F10 mouse model of melanoma is a widely used model to study many aspects of cancer biology and therapeutics in a solid tumor. Melanomas aggressively progress within a dynamic microenvironment containing in addition to tumor cells, stroma cells and components such as fibroblasts, immune cells, vascular cells, extracellular matrix (ECM) and extracellular molecules. The goal of this study was to elucidate the processes of tumor progression by identifying differentially expressed proteins in the tumor mass during specific stages of tumor growth. A comparative proteome analysis was performed on B16-F10 derived tumors in C57BL/6 mice at days 3, 5, 7, and 10. Statistical approaches were used to determine quantitative differential protein expression at each tumor time stage. Hierarchical clustering of 44 protein spots ($p < 0.01$) revealed a progressive change in the tumor mass when all 4 time stages were classified together, but there was a clear switch in expression of these proteins between the day 5 and the day 7 tumors. A trend analysis showed 53 protein spots ($p < 0.001$) following 6 predominant kinetic paths of expression as the tumor progressed. The protein spots were then identified using MALDI-TOF mass spectrometry. Proteins involved in glycolysis, inflammation, wounding, superoxide metabolism, and chemotaxis increased during tumorigenesis. From day 3 to day 7 VEGF and active cathepsin D were induced 7-fold and 4-fold, respectively. Proteins involved in electron transport, protein folding, blood coagulation, and transport decreased during tumorigenesis. This work illustrates changes in the biology of the B16-F10 tumor mass during tumor progression.

Keywords: proteomics • melanoma • tumor progression • Cathepsin D • albumin • VEGF

Introduction

B16-F10 is a mouse melanoma cell line that when subcutaneously (s. c.) injected into the flanks of C57BL/6 mice forms aggressively progressing solid tumors. This tumor model has been widely used to study the spectrum of cancer biology including oncogenes and tumor suppressor genes,[1−3] protein−protein interactions,[4] and complex biological processes such as angiogenesis and metastasis.[5,6] Additionally, this model has been used to study therapeutics for solid tumors, such as pharmacological compounds,[7] immunotherapy,[8,9] and interfering RNAs.[10]

Solid tumors progress in a microenvironment consisting of in addition to tumor cells, nontumor cells, extracellular matrix components (ECM), e.g., collagens and elastins, and soluble components, e.g., cytokines, chemokines, and growth factors, and during tumor progression the relative abundance and presence of these constituents are likely changing.[11] The nontumor cells, or stromal cells, include fibroblasts, endothelial cells, fat cells, and immune cells, and they are involved in tumor progression through tumor-stroma interactions in three predominant forms: (1) extracellular soluble factors, (2) intracellular communication via second messengers and signal transduction networks, and (3) intercellular communication via cell−cell adhesion and gap junctions.[12] Currently, there are many therapeutics targeting the tumor-stroma interactions including adhesion molecules, proteases, signaling pathways, and ECM components.[13] Discovering new therapeutic targets from tumor microenvironment constituents, and not just tumor cells, is an enticing approach for solid tumor therapeutics. However, the level of complexity is dramatically increased because different cell types are present in the tumor mass resulting in an increase in the number of proteins that need to be evaluated. Studying the tumor as it progresses in vivo, and using large scale -omics technologies may reveal new molecular targets.

Since proteins are involved in structure and catalysis in tissues, and because they are the most commonly targeted molecule for therapeutics, a kinetic proteome analysis was done on the B16-F10 solid tumor. In this study, the whole tumor

* To whom correspondence should be addressed. Protein Biochemistry Section, National Eye Institute, National Institutes of Health, 7 Memorial Drive, Building 7 Room 237, Bethesda, MD 20892. Tel: (301) 496-6806. Fax: (301) 496-1759. E-mail: culpd@nei.nih.gov.

† National Institutes of Health.

‡ Tumor Research Institute.

§ Karolinska Hospital/Institute.

Published on Web 05/09/2006

10.1021/pr060059q CCC: $33.50

mass proteome was analyzed including any circulating fluids, e.g., blood contained in tumor vasculature. We used high resolution 2D gel electrophoresis for protein separation followed by mass spectrometry for protein identification. To obtain quantitative data on differentially expressed proteins we used new image analysis software, Ludesi's 2D Analyzer and the informatics software, 2D Interpreter. Also, a Jonckheere–Terpstra test[14] was performed to show ordered differences between the time stages to reveal protein expression trends within the progressing tumors. We validated our findings from the comparative proteomic study by probing for specific cell types and proteins that correlate with the biological processes associated with the proteins identified. This was a discovery based proteomics study to identify differentially expressed proteins during tumor progression in a widely used mouse model of solid tumors.

Materials and Methods

Animals and Cell Line. Female C57BL/6 mice (6–8 weeks) were purchased from Taconic Farms (Rockville, MD), and cared for in accordance with the guidelines set forth by the Animal Research Advisory Committee of the National Institutes of Health (NIH). The NIH is accredited by the American Association for the Accreditation of Laboratory Animal Care. B16-F10, a melanoma cell line of C57BL/6 origin, was cultured in T-225 tissue culture flasks in Iscove's Modified Dulbecco's Medium (Cambrex, Walkersville, MD), 10% heat-inactivated fetal bovine serum (Invitrogen, Carlsbad, CA), 2 mM glutamine (Invitrogen), 100 Units/ml penicillin/100 μg/mL streptomycin (Invitrogen), and 2.5 μg/mL fungizone-amphotericin B (Cambrex). The cells were cultured to 95% confluency at 37 °C with 5% CO_2 and humidity, and harvested by washing the flask once with sterile PBS and then incubating with 3 mL trypsin/versene (Invitrogen) for 5 min at 37 °C. The harvested cells were washed twice in PBS, resuspended at 2×10^7 cells/ml in PBS, and 100 μL was injected subcutaneously (s. c.) into mice.

Tissue Specimens. Both flanks on C57BL/6 mice were shaved and injected with tumor cell suspensions the same day. Animals were euthanized using CO_2 on days 3, 5, 7, and 10 after tumor challenge. Tumor volume was measured by multiplying length $\times$ width $\times$ height divided by 2. Immediately after euthanasia, the entire tumor mass was carefully dissected excluding any extraneous host tissue, frozen on dry ice, and stored at −80 °C until analyzed. The 2 tumors from each mouse were pooled, weighed, and homogenized on ice using a glass tissue grinder. For every 2 mg of tissue, 1 μL of 0.5M EDTA, 10 μL protease inhibitor cocktail (Sigma, Milwaukee, WI), and 100 μL lysis buffer (9M urea containing 4% CHAPS, and 15 mg/mL dithiothreitol (DTT)) were added. The homogenates were centrifuged at 16 000 $\times$ *g* for 20 min. Protein concentrations of the soluble fractions were determined by 1D gel electrophoresis using NuPAGE Novex Bis-Tris Gels, and a Colloidal Blue Staining Kit (Invitrogen). 1D gels were scanned on a Molecular Dynamics Personal densitometer, and the protein concentrations were quantified by generating a standard curve using bovine serum albumin (BSA) (2 mg/mL, Pierce, Rockford, IL). The samples were stored at −80 °C prior to 2D-PAGE.

2D Polyacrylamide Gel Electrophoresis (2D PAGE). The first dimension isoelectric focusing was performed using the IPGphor and nonlinear, pH 3–10, 180 mm $\times$ 3 mm $\times$ 0.5 mm DryStrips (GE Healthcare, Piscataway, NJ) following the manufacturers instructions. Briefly, in 350 μL total volume, 200 μg of protein was loaded during rehydration of the strips in 8M urea solution containing, 2% CHAPS, 2.5 mg/mL DTT, 0.5% pH 3–10 IPG buffer. The proteins were focused for 28 000 Vhrs. The strips were frozen at −80 °C for 24 h, and subsequently equilibrated first in Tris pH 8.8 buffer containing 6 M urea, 2% SDS and 8.6 mg/mL DTT for 15 min followed by 15 min in the same buffer containing 43 mg/mL iodoacetamide. An acrylamide gradient of 15–18% was used with 20 $\times$ 25 cm gels for the second dimension. Proteins were fixed in 50% ethanol with 1% phosphoric acid for a minimum of 12 h. The gels were washed 3$\times$ in deionized water, stained for 3 days with colloidal Coomassie Blue G-250,[15] and washed in deionized water for at least 24 h to clear the background. The images were collected using the Molecular Dynamics Personal densitometer.

Image Analysis and Statistics. Gel images were analyzed by Ludesi using their 2D Analyzer software (Lund, Sweden). The automatically generated spot detection, segmentation, and matching were checked manually by us for accuracy. For each time stage at days 3, 5, 7, and 10, we independently analyzed tumors from 2, 3, 3, and 4 mice, respectively. Gels were run in triplicate for each mouse when tumor size allowed. Averaged gels were generated from replicates done per mouse to minimize technical variance. The volume for each spot on an averaged gel was calculated as the sum of the normalized volumes of a spot on a set of gels divided by the number of gels used to generate the average.

Quantitative differential protein expression among the 4 groups (days 3, 5, 7, and 10) was assessed by us using Ludesi's 2D Interpreter. Analysis of variance (ANOVA) with p-values < 0.05 was used for selecting proteins from the averaged gels among the mice in each group for subsequent statistical analysis. ANOVA treated a missing spot as zero; therefore, all spots within each group were evaluated. Support Vector Machines (SVMs) and hierarchical clustering (HC) were used to classify those proteins selected by ANOVA. For SVM analysis, the polynomial degree was 1, the data were normalized. The degree of similarity for the HC analysis was measured by the Pearson Correlation distance function with an average linking method.

Three independent classifications (day 3 to day 5, day 5 to day 7, day 7 to day 10) using SVMs and HC were performed on the ANOVA ($p < 0.05$) selected proteins. We used a random 75% of the mice in each group to train a data set of spots selected by ANOVA, and all mice were tested. In the day 3 to day 5 and day 5 to day 7 classifications the training and test data were the same, thus only proteins with an acceptable ANOVA score were characterized as differentially expressed. The day 7 to day 10 classification had four mice in the day 10 group, therefore, three day 10 mice were used to train and four day 10 mice were tested. For this classification, proteins that had an acceptable ANOVA score and that correctly placed day 10 mice together were characterized as differentially expressed. A fourth classification was done to analyze all four groups at once using ANOVA selected spots ($p < 0.01$). This approach identified 44 proteins that allowed the correct classification of each mouse into their respective groups (i.e., 3, 5, 7, and 10). To test if these proteins would correctly place mice into their respective groups using less than 75% training data, we manually selected the training data as follows: train and test with two mice in the day 3 group, train with two mice and test three mice in the day 5 and day 7 groups, and train with two mice and test four mice in the day 10 group. Mice were correctly classified in this analysis.

A Jonckheere–Terpstra (J–T) test was performed to identify protein spot trends as the tumor grew in vivo. The J–T test

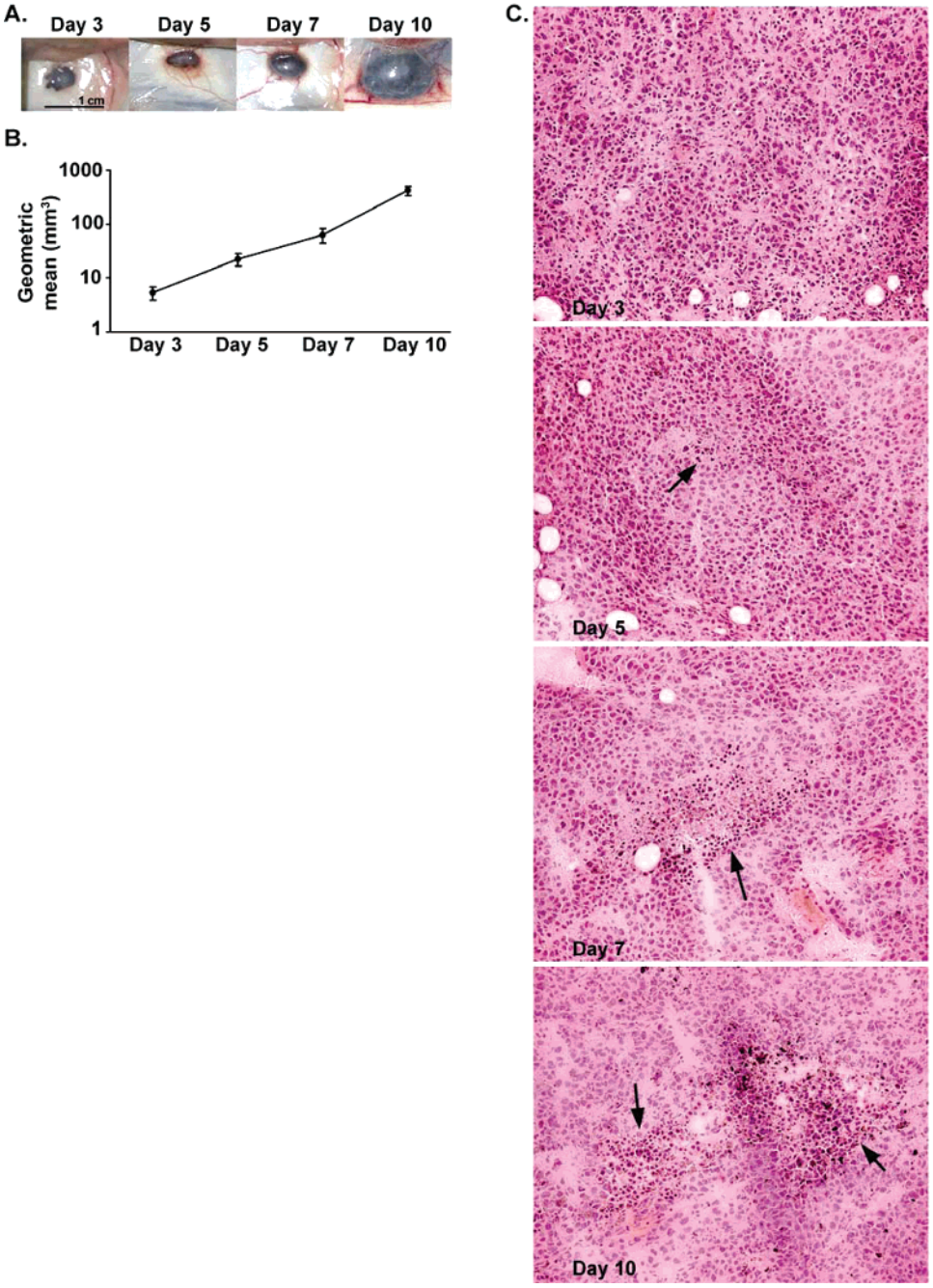

Figure 1. Tumors in C57BL/6 mice after challenging with suspensions of 2×10^6 B16-F10 mouse melanoma cells. (**A**) In vivo photographs of the tumors at days 3, 5, 7, and 10 representing more than 8 tumors at each time point. (**B**) Four mice per group were challenged subcutaneously and bilaterally (2 tumors per mouse). Tumors from each mouse were pooled for the analysis (days 3, 5, 7, $n = 8$ tumors, day 10 $n = 7$ tumors). The tumors on a mouse at the day 10 time point merged and the measurement was taken on this larger single tumor. The tumor volume is plotted. (**C**) Hematoxylin and eosin staining on days 3, 5, 7, and 10 B16-F10 tumors (20× lens magnification). Black arrows indicate areas of necrosis in the tumor mass.

evaluates ordered differences among independent samples, for example, mean value of day 3 ≤ mean day 5 ≤ mean day 7 ≤ mean day 10 for a given protein spot. The J−T test is a two sided test, therefore the opposite was also tested, mean value of day 3 ≥ mean day 5 ≥ mean day 7 ≥ mean day 10. Twelve different orderings were tested, and to minimize false positives a low significance value was used ($p < 0.001$).

Trypsin Digest and Mass Spectrometry. Protein spots were excised from the 2D gels and destained with 50% ethanol and 50 mM NH_4HCO_3 at room temperature (RT). Gel pieces were dehydrated in acetonitrile (ACN), dried in a Speedvac, and subjected to in-gel digestion by rehydration with 10 ng/μL modified trypsin (Promega, Madison, WI, and Sigma) and 50 mM NH_4HCO_3. Protein digestion was for an average of 18 h at RT. Tryptic peptides were extracted by washing twice; first in 50% ACN and 1% formic acid followed by 95% ACN and 5% formic acid. Extracted peptides were lyophilized and stored at −20 °C until analysis. The peptides were spotted onto a steel target with α-cyano-4-hydroxycinnamic acid in 50% ACN containing 1% formic acid or 0.5% trifluoroacetic acid. The peptide masses were determined on an Applied Biosystems Voyager System DE-STR MALDI-TOF mass spectrometer with

delayed extraction. The instrument was calibrated with trypsin digested, horse apomyoglobin over a mass range of 300−2000 Da and recalibrated as necessary to maintain 50 ppm accuracy. Trypsin autolysis peaks were used for internal calibration. The instrument parameters were set as follows: extraction delay time of 280 ns, grid voltage 70%, and an initial acceleration voltage of 20 000 V with 50 nitrogen laser shots accumulated per sample spectrum. Measured mass spectra were noise filtered (correlation factor 0.7) and baseline corrected using Data Explorer (v. 4.0.0.0). Monoisotopic peaks were identified manually, by Mascot Wizard (Matrix Science, v. 1.1.2.0), or by *m*/*z* (Genomic Solutions, Ann Arbor, MI) and catalogued for data analyses. The Mascot (Matrix Science, v. 1.9) or ProFound (Genomic Solutions, v. 4.10.5) search algorithms were used to analyze the peptide mass fingerprinting data. Acceptable protein identifications required a Mascot Mowse score greater than 60, and an expect score of less than 0.1. Acceptable protein identifications for both Mascot and ProFound required a delta mass less than 0.1 Da or 0.03% for each peptide matched, and a minimum of 5 peptides except where indicated. The NCBInr database was used for the searches.

Immunoblotting. Proteins were separated by 1D gel electrophoresis, and transferred to 0.2 μm polyvinylidine difluoride membrane (Millipore, Billerica, MA). Primary and secondary antibodies were diluted into PBS (Invitrogen) containing 0.1% Tween 20 (Sigma) and 5% nonfat dried milk (Bio-Rad). Primary antibodies used included goat biotinylated anti-mouse Cathepsin D (1: 250, R&D Systems, Minneapolis, MN), and rabbit anti-VEGF (A-20) (1:100, Santa Cruz Biotechnology, Santa Cruz, CA). Horseradish Peroxidase conjugated anti-biotin (1:500, Cell Signaling Technology, Danvers, MA) and anti-Rabbit (1:3000, GE Healthcare) secondary antibodies were used with GE Healthcare's enhanced chemiluminescence (ECL) detection kit. Chemiluminescence was detected with a Nikon CCD camera.

Immunohistochemistry. Unfixed frozen tumors for each time point were sectioned and stained with hematoxylin and eosin. All immunohistochemistry incubation steps were performed in a moist chamber. Sections were fixed for 10 min in PBS containing 4% formaldehyde, and rinsed 3 times with PBS. Endogenous peroxidases were inactivated by incubating the sections for 30 min in deionized water containing 5% hydrogen peroxide, and rinsed once with deionized water. Sections were washed 2 × 5 min in TBS, blocked for 20 min in TBS containing 1% normal rabbit serum (Vector Laboratories, Burlingame, CA), rinsed once with TBS, and incubated overnight at 4 °C with the primary antibody. Rat anti-mouse CD31 (monoclonal; BD Biosciences, San Jose, CA), and rat anti-mouse CD68 (monoclonal; Serotec, Raleigh, NC) were used at 1:100 dilutions in TBS with 1% BSA. Negative controls were with no primary antibody. Sections were washed 3 × 10 min in TBS, and incubated for 30 min in a 1:200 rabbit biotinylated anti-rat IgG (H+L), mouse adsorbed (Vector Laboratories) secondary antibody. Sections were washed 3 × 3 min in TBS, incubated for 30 min in the VECTASTAIN Elite ABC Reagent (Vector Laboratories), washed 3 × 10 min and incubated for 5 min in TBS containing 0.6 mg/mL of the peroxidase substrate, 3.3′-Diaminobenzidine tetrahydrochloride (Sigma), and 0.03% hydrogen peroxide added just before use. All sections were counterstained with hematoxylin.

Results

B16-F10 Tumor Growth in Mice. Representative tumors depicting growth at days 3, 5, 7, and 10 after subcutaneous injection of B16-F10 are shown in Figure 1. The day 3 established tumors were flat, with only trace vascularization seen around the tumor. By day 5, the tumors grew vertically, vascularization was visible, and the tissue surrounding the tumor was discolored, potentially indicating the presence of inflammation. The day 7 tumors continued to develop in both the horizontal and vertical planes, showing increased vascularization. The day 10 tumors were very large and vascularized. The geometric mean of the tumor volume at each time point was plotted on a logarithmic scale (Figure 1B), and demonstrates the reproducibility of growth in this solid tumor model. Hematoxylin and eosin staining on the progressing tumors at each time point was performed to determine the relative contribution of stromal cells to the tumor mass (Figure 1C). The tumor mass contained >90% tumor cells in all time stages, suggesting that most proteins were of tumor cell origin. A progressive increase in necrosis was observed within the tumor tissue indicated by the black arrows in Figure 1C. The day 5 tumor had small patchy areas of necrosis, and by day 10 large areas of necrosis were visible. Unlike the day 5 and day 7 tumors, sections of the day 10 tumors contained patches of melanin that were associated with areas of necrosis.

Quantitative Differential Protein Expression in Progressing B16-F10 Tumors. High resolution 2D gel electrophoresis was done on the tumor proteins and a representative gel is shown in Figure 2. The average number of protein spots detected at each time point increased as the tumor progressed (day 3−869, day 5−1210, day 7−1424, and day 10−1538). 2D Interpreter was used to determine quantitative differentially expressed proteins between time points of the progressing B16-F10 tumors. Since at each time point, >90% of the cells were tumor cells, to detect changes in protein expression that may be contributed by stroma components as well as subtle changes in the tumor cells, it seemed necessary to be able to confidently detect low fold changes in protein expression. The day 3 to day 5, day 5 to day 7, and day 7 to day 10 tumors had 46, 58, and 15 ($P < 0.05$) differentially expressed spots, respectively, using approaches described in the methods. Fold changes in protein expression ranged from 1.4 to 6.8, indicating that very small changes in protein expression were significant and detectable in our system. For a few proteins that were very reproducibly present on the gels, statistically significant changes of 1.2 were determined (data not included). The positions on a gel for differentially expressed proteins identified by MALDI-TOF mass fingerprinting are indicated in Figure 2, and in Table 1 are the most probable identities of those proteins determined by the MALDI-TOF mass spectra.

Classification of All Four Time Stages. Hierarchical clustering and Support Vector Machines on ANOVA selected protein spots from all mice were done. The differential expression of 44 proteins correctly classified the mice into their respective groups. In addition, when a heat map of the relative expression of these 44 protein spots was plotted (Figure 3A), a progressive change was clear, but a marked switch in protein expression was obvious between the day 5 and the day 7 time stages. Of the 44 proteins, 31 proteins were down regulated and 13 proteins were up regulated from day 5 to day 7. Shown in Figure 3B are the identifications of those proteins associated with the switch between day 5 and day 7; 13 were murine albumin, and in Table 2 the span of peptides observed for albumin from the MALDI-TOF peptide mass fingerprinting data and the estimated molecular mass

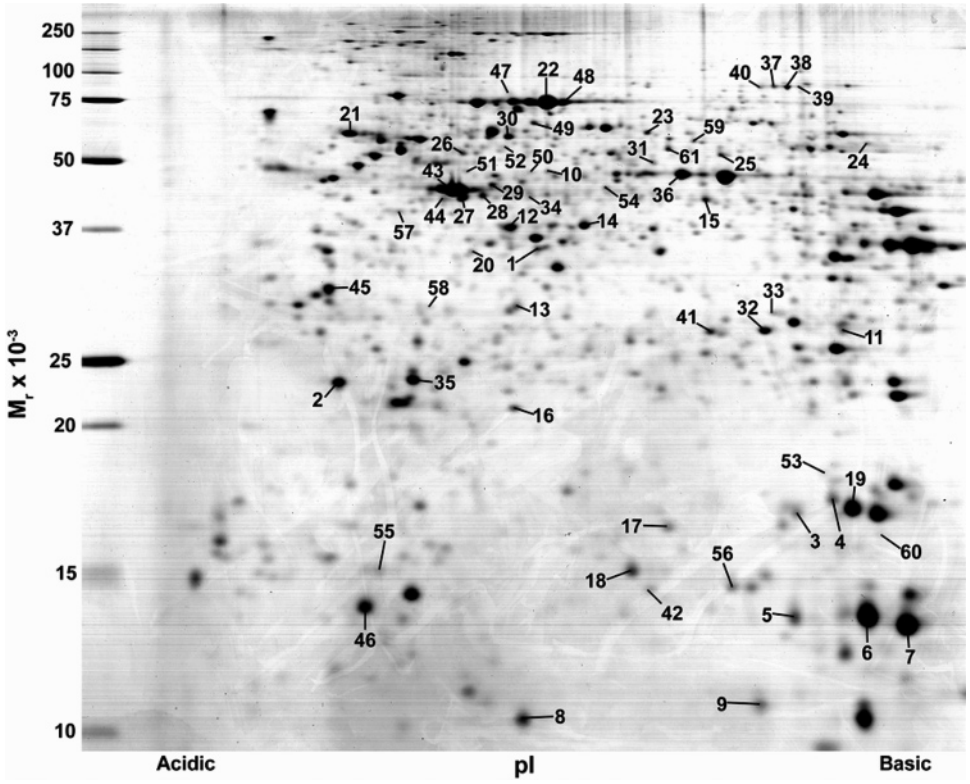

Figure 2. 2D acrylamide gel of day 7 tumor proteins representing 8 gels. Proteins were focused over an IPG pH gradient of 3−10, separated in a 15−18% polyacrylamide gradient and stained with colloidal Coomassie. Protein spots identified by MALDI-TOF mass spectrometry are numbered, and correspond with proteins identified in Tables 1 and 2 and Figures 3 and 4.

from those residues are shown. The latter are generally very similar to the relative molecular weight estimated from gel migration.

Trend Analysis of Protein Spots in Progressing B16-F10 Tumors. The 3 classifications of the tumor growth kinetics described above (day 3 to day 5, day 5 to day 7, and day 7 to day 10) revealed trends of protein spot expression that were both continuous and sporadic. Thus, a Jonckheere−Terpstra (J−T) test was performed to identify protein spot trends for all time stages. *P*-values were calculated using averaged gel spot volumes, and if a spot was not present in 2 or more of the time stages, it was not used. Six predominant trends were identified, and a total of 53 protein spots ($p < 0.001$) fit into the trends. Trends 1 and 2 represented a continuous increase or decrease in protein expression, respectively. Eight spots fit into Trend 1, and 14 spots fit into Trend 2. Notably, 10 of 14 spots in Trend 2 were albumin. Four spots fit into Trend 3, which shows protein expression increases from day 5 to day 10 (Figure 4A unknown protein). Eight spots fit into Trend 4, which shows protein expression decreases from day 3 to day 7 (Figure 4A transferrin). Ten spots fit into Trend 5, which shows protein expression increases from day 3 to day 7 and plateaus or shows a small decrease at day 10 (Figure 4A prohibitin). Nine spots fit into Trend 6, which shows protein expression is up or goes up from day 3 to day 5 and then decreases from day 5 to day 10 (Figure 4A calgranulin A). Identified proteins that fit into a particular trend are shown in Figure 4B.

Macrophages and Endothelial Cells Populate Progressing B16-F10 Tumors. The necrotic tumor tissue seen at later time stages (Figure 1C) suggested that phagocytic cells may be infiltrating and localizing to these areas of the tumor mass. We stained tumor sections for macrosialin, (CD68) a macrophage specific protein that is typically localized intracellularly in late endosomes.[16] In Figure 5A, the day 3 tumor had trace staining for the macrosialin protein. By day 7, cells within the tumor had an increase in staining indicating there was an infiltration of CD68 positive cells. These cells were most prominent around the areas of necrosis (Figure 5A, black arrow).

Tumors require nutrients and oxygen via angiogenesis to sustain growth.[17] To assess the angiogenic progression of B16-F10 tumors, we stained tumor sections for CD31, a membrane protein that is constitutively expressed on the surface of endothelial cells of blood vessels.[18] Few CD31 positive cells were seen in the day 3 tumor; they were present in the striated skeletal muscle and on the periphery of the tumor (Figure 5A). By day 7, blood vessels had formed throughout the tumor, indicated by CD31 positive staining, and they were commonly associated with the areas of necrosis (black arrow, Figure 5A). The sections were also stained with vascular endothelial cadherin (VE-cadherin), another endothelial cell-specific marker of blood vessels, and confirmed the blood vessel development in the tumors (data not shown). We also assessed the onset of angiogenesis by immunoblotting for vascular endothelial growth factor (VEGF), a protein induced during early tumorigenesis.[19] The B16-F10 tumor cells and the day 3 tumor tissue showed no VEGF expression (Figure 5B). However, 2 bands were exposed in the days 5, 7, and 10 tumors, and both bands were used for quantitative analysis. VEGF expression was induced 4.2-fold between day 3 and day 5, 3.3-fold between day 5 and day 7, and reduced 1.5-fold between day 7 and day 10. VEGF expression also follows Trend 5 (Figure 4A).

Cathepsin D is Increased in the B16-F10 Tumor Mass. Cathepsin D is a lysosomal aspartic protease that is thought

Table 1. MALDI-TOF Identification of Regulated Proteins[a,b,c,d,h]

spot	protein	acc. no.	theoretical M_r (x10^{-3})/p*I*	peptides matched/ searched	percent coverage	Mowse score	expect score	fold change
			up-regulated proteins					
	day 3 to day 5							
1	Pyruvate kinase, isozyme M2	P52480	58/7.2	7/25	18	69	0.011	1.6
2	Translationally controlled tumor protein	AAH86358	19/4.8	9/32	32	103	4.0e-06	1.8
3	RNA binding motif protein 3	AAH06580	17/6.8	8/34	44	87	0.00015	1.7
4	Nucleoside diphosphate kinase B	NP_032731	17/7.0	9/21	55	118	1.3e-07	1.4
5	Calgranulin B	NP_033140	13/6.6	5/9	38	n/a	0.015	2.0
6	Hemoglobin beta	690944A	16/7.3	5/9	45	82	0.0021	2.9
7	Hemoglobin alpha	AAH43020	15/8.0	6/10	54	78	0.0012	1.9
8	Calgranulin A[e]	P27005	10/5.4	3/9	73	65	0.0037	2.3
9	Hemoglobin, beta adult major chain	NP_032246	16/7.1	9/34	57	78	0.0013	6.8
10	Albumin 1	NP_033784	71/5.8	13/18	28	n/a	<0.01	2.1
11	Adenylate kinase 2	NP_058591	26/7.0	6/19	27	n/a	<0.01	1.8
	day 5 to day 7							
11	Adenylate kinase 2	NP_058591	26/7.0	6/19	27	n/a	<0.01	2.5
12[f]	Eukaryotic translation initiation factor 3, subunit 2 (beta)/Enolase 1, alpha nonneuron	NP_061269/ AAH85098	37/5.4/47/6.4	7/29/8/29	24/23	62/71	0.046/0.0059	1.4
13	Prohibitin	NP_032857	30/5.6	14/66	61	152	5.3e-11	1.5
14	Phosphoglycerate kinase 1	NP_032854	45/7.5	16/55	40	126	2e-08	2.0
15	Enolase 1, alpha nonneuron	AAH85098	47/6.4	12/74	37	74	0.0028	1.6
16	ATP synthase, H+ transporting, mitochondrial F0 complex subunit d	AAH81431	19/5.5	9/41	57	87	0.00016	1.4
17	Superoxide dismutase 1	NP_035564	16/6.0	8/29	42	104	3.2e-06	1.4
18	Fatty acid binding protein 5, epidermal	NP_034764	15/6.0	10/64	46	96	2.1e-05	1.9
19	Peptidylprolyl isomerase A	NP_032933	18/7.7	9/42	61	100	8.2e-06	1.5
20	Pyrophosphatase	NP_080714	33/5.4	8/19	31	n/a	5.2e-05	1.4
	day 7 to day 10							
6	Hemoglobin beta	690944A	16/7.3	5/9	45	82	0.0021	2.4
			down-regulated proteins					
	day 3 to day 5							
21	Prolyl 4-hydroxylase, beta polypeptide	NP_035162	57/4.8	14/72	27	80	0.00086	1.6
22	Albumin 1[g]	NP_033784	71/5.8	23/63	44	107	1.6e-06	2.1
23	Fibrinogen, B beta polypeptide	NP_862897	55/6.7	10/21	23	73	0.017	1.8
24	Fibrinogen, B beta polypeptide	NP_862897	55/6.7	17/24	32	n/a	<0.01	1.6
25	Aldehyde dehydrogenase 2	AAH05476	57/7.7	14/20	33	n/a	9.8e-11	1.4
	day 5 to day 7							
5	Calgranulin B	NP_033140	13/6.6	5/9	38	n/a	0.015	1.7
10	Albumin 1	NP_033784	71/5.8	13/18	28	n/a	<0.01	2.6
22	Albumin 1[g]	NP_033784	71/5.8	23/63	44	107	1.6e-06	2.2
26	Albumin 1	NP_033784	71/5.8	8/14	14	61	0.067	1.6
27	Albumin 1	NP_033784	71/5.8	12/17	22	151	6.7e-11	4.0
28	Albumin 1	NP_033784	71/5.8	12/48	20	82	0.00047	1.6
29	Albumin 1	NP_033784	71/5.8	30/82	42	122	5.1e-08	1.8
30	Albumin 1	NP_033784	71/5.8	19/37	34	120	8.0e-08	1.6
31	Albumin 1	NP_033784	71/5.8	10/20	21	66	0.018	2.9
32	Albumin 1	NP_033784	71/5.8	9/17	18	68	0.014	1.7
33	Albumin 1	NP_033784	71/5.8	10/16	19	n/a	<0.01	2.0
34	Albumin 1	NP_033784	71/5.8	13/17	23	n/a	<0.01	3.6
35	Albumin	CAC81903	24/5.5	10/45	47	78	0.0052	1.6
36	Enolase 1, alpha nonneuron	AAH85098	47/6.4	16/44	43	153	4.0e-11	1.7
37	Transferrin	NP_598738	79/6.9	14/31	22	77	0.0017	3.4
38	Transferrin[g]	NP_598738	79/6.9	15/33	25	77	0.0015	3.2
39	Transferrin	NP_598738	79/6.9	19/25	28	n/a	5.5e-14	2.9
40	Transferrin	NP_598738	79/6.9	20/27	30	n/a	1.2e-14	2.6
41	Proteasome subunit, alpha type 6	NP_036098	28/6.3	8/17	33	80	0.00075	1.7
42	Transthyretin	AAH24702	16/5.8	7/12	44	n/a	2.3e-06	2.0
	day 7 to day 10							
2	Translationally controlled tumor protein	AAH86358	19/4.8	9/32	32	103	4.0e-06	1.3
8	Calgranulin A[e]	P27005	10/5.4	3/9	73	65	0.0037	3.0
20	Pyrophosphatase	NP_080714	33/5.4	8/19	31	n/a	5.2e-05	1.4
43	Gamma-actin[g]	CAA31455	41/5.6	12/45	32	76	0.0018	1.3
44	Albumin 1	NP_033784	71/5.8	12/28	21	115	2.7e-07	2.7
45	Tropomyosin 3[g]	NP_071709	33/4.7	9/26	16	43	3.7	1.4
46[f]	Thioredoxin 1/Parvalbumin	NP_035790/ NP_038673	12/4.8/12/5.0	9/54/9/54	72/52	104/90	3.2e-06/8.6e-05	1.3

Table 1 (Continued)

spot	protein	acc. no.	theoretical M_r (x10^{-3})/pI	peptides matched/ searched	percent coverage	Mowse score	expect score	fold change
			other identified proteins					
47	Hemopexin	AAB49490	51/7.3	15/46	31	95	0.0001	n/a
48	Albumin 1	NP_033784	71/5.8	17/43	31	93	4.1e-05	n/a
49	Albumin 1	NP_033784	71/5.8	8/18	17	51	0.59	n/a
50	Albumin 1	NP_033784	71/5.8	11/11	21	n/a	<0.01	n/a
51	Albumin 1	NP_033784	71/5.8	11/12	18	n/a	<0.01	n/a
52	Albumin 1	NP_033784	71/5.8	911	17	n/a	<0.01	n/a
53	Albumin 1	NP_033784	71/5.8	7/7	14	n/a	<0.01	n/a
54	Gamma-actin	CAA31455	41/5.6	13/50	32	86	0.00022	n/a
55	Alpha-cardiac actin	AAA37166	17/5.3	6/16	40	n/a	<0.01	n/a
56	Histidine triad nucleotide binding protein 1	NP_032274	14/6.4	5/11	52	n/a	0.011	n/a
57	Serine/threonine kinase receptor associated protein	NP_035629	39/5.0	9/19	38		<0.01	n/a
58[f]	Chloride intracellular channel 1/Serum albumin − mouse (fragment)	NP_254279/ A05139	27/5.1/53/5.5	6/13/5/7	28/15	n/a	<0.01/4.8e-03	n/a
59	3-phosphoglycerate dehydrogenase	AAH86668	57/6.1	6/15	16	n/a	1.4e-03	n/a
60	Peroxiredoxin 5	AAG13450	17/7.8	6/6	48	n/a	7.1e-06	n/a
61	Chaperonin subunit 2 (beta)	AAH26918	58/6.0	21/62	49	121	6.4e-08	n/a

[a] Spot numbers correspond with the gel image in Figure 2. [b] Albumin was identified in 20 spots each migrating at a different M_r and pI. Albumin is synthesized as a 608 aa preproprotein, containing a signal sequence at residues 1−18, a propeptide from residues 19−24, and albumin from 25 to 608. Spots 35 and 58 are fragments of the preproalbumin and are cataloged separately in the NCBInr database. [c] Mascot provided a Mowse score and an expect score and Profound only provided an expect score. [d] Spots 45 and 49 were manually validated to confirm the identification. [e] Three peptides were accepted for calgranulin A because of high protein coverage. [f] Two proteins were identified from one spot, and there were no identifying peptides present in both identifications. [g] Peptide mass tolerance ± 0.5 Da. [h] n/a − not applicable.

to have a role in cancers and is the major enzyme that degrades denatured serum albumin in mouse liver and kidney lysosomes.[20] Cathepsin D is synthesized as a prepro-enzyme and after proteolytic cleavages produces the active form of the protein (42 kDa). The protein undergoes further proteolytic cleavage into heavy (30 kDa) and a light (13 kDa) chains under denaturing conditions.[21] Immunoblots for cathepsin D showed a 2.9-fold increase between day 3 and day 5 and a 1.5-fold increase between day 5 and day 7 and between day 7 and day 10, respectively, in the active form of the protein (Figure 5B). B16-F10 cell lysates contained only the active form of the protein, but at levels similar to the day 7 and day 10 tumors.

Discussion

This study was a kinetic proteome analysis of 4 stages in the progression of the aggressive B16-F10 mouse melanoma model from the flat, radial growth of newly established tumors to the onset of vascularization and vertical growth of well vascularized tumors. In this study, we used statistical approaches to identify quantitative differentially expressed proteins. Thus, our inclusion criteria were based on the quality and reproducibility of the data, making it possible to identify those proteins with a very low fold change. The importance of identifying small changes in biological systems may be very significant, particularly during tumor progression where small changes in enzymes may have large biological effects, and since these tumors were >90% tumor cells, large changes in the stroma will still be seen as small relative changes in protein expression. The heat map of the differential expression of 44 proteins (Figure 3A) of unknown origin correlated with changes in the tumor microenvironment, as demonstrated by increased vascularization and albumin catabolism. Additionally, these proteins suggest that there were significant changes in tumor cell metabolism. This proteomic approach allowed us to visualize protein expression changes within an evolving tumor that reflect in vivo processes of tumor progression.

The dramatic drop in concentrations of many albumin intermediates (Table 2) indicated there was a major change in the degradation of albumin at the day 5 to day 7 transition. Albumin is synthesized almost exclusively in the liver, and is the most abundant protein in the blood making up 2.5−4.8 g per 100 mL in the mouse. The decrease in albumin in these tumors is not a systemic effect due to the large tumor burden, because a mouse serum profile revealed that tumor bearing mice at all time stages were not hypoalbuminemic (data not shown). In normal animals, one of the major sites of albumin catabolism is the skin.[22] Interestingly, in tumor bearing animals and humans, it has been shown that tumors accumulate albumin, and it is thought that tumors become a major site of albumin catabolism.[23] In our study, B16-F10 cell lysates have no detectable mouse albumin, as determined by antibody reaction (data not shown). Also by antibody reaction, mouse albumin was detected at all time stages and correlated with the image analysis data, but between day 5 and day 7 as seen in Table 1, Figure 3B and Figure 4B, there is a significant decrease in 20 forms of the protein. The decrease in albumin is at a time when there is an increase in the vascularization of the tumor, and one would expect higher concentrations of albumin not a decrease in all forms of albumin. Thus, the results are consistent with the proposal that albumin and other plasma proteins, such as transthyretin, are a major energy and nitrogen source for tumors.[24] As seen in Figure 3A transthyretin is also decreased between day 5 and day 7.

The enzyme that has been shown to be the major protease responsible for degrading albumin in lysosomes is cathepsin D.[20] However, the optimal pH for the enzyme is 3 which is lower than the pH within lysosomes. Cathepsin D will proteolyze denatured albumin at pH 4−5, and the enzyme cleaves between hydrophobic sites.[25] It is not clear if the albumin species found in the B16-F10 tumors are generated by cathepsin D catalysis, but 9 of the 13 albumin forms identified in the switch (Figure 3*A*) consisted of only domains: 4 contained

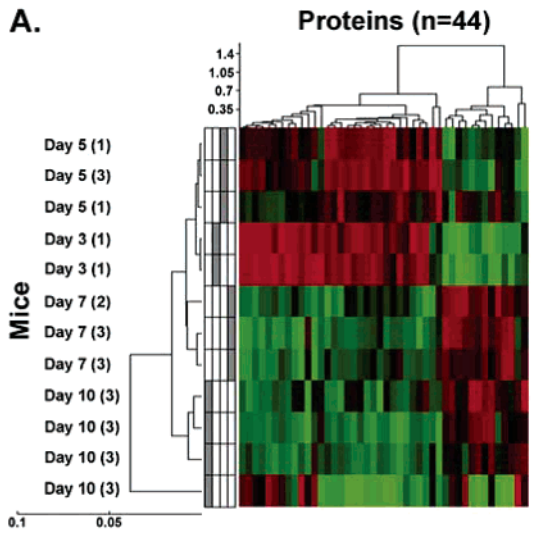

B.

Proteins up regulated between day 5 and day 7

Pyruvate kinase, isozyme M2 (1)
Translationally-controlled tumor protein (2)
Eukaryotic translation initiation factor 3, subunit 2 (beta) (12)
Enolase 1, alpha non-neuron (12, 15)
Prohibitin (13)
Phosphoglycerate kinase 1 (14)
Fatty acid binding protein 5, epidermal (18)
Alpha-cardiac actin (55)
Histidine triad nucleotide binding protein 1 (56)
Serine/threonine kinase receptor associated protein (57)

Proteins down regulated between day 5 and day 7

Calgranulin A (8)
Albumin 1 (10, 22, 26, 27, 28, 29, 30, 32, 33, 34, 44, 48, 50)
Enolase 1, alpha non-neuron (36)
Prolyl 4-hydroxylase, beta polypeptide (21)
Fibrinogen, B beta polypeptide (23, 24)
Aldehyde dehydrogenase 2 (25)
Transferrin (37, 38, 39, 40)
Transthyretin (42)
Hemopexin (47)

Figure 3. (**A**) Heat map of all 4 groups (days 3, 5, 7, and 10) demonstrating a switch in protein expression of 44 proteins between day 5 and day 7. Spots for Support Vector Machines and hierarchical clustering analysis were selected by ANOVA ($p < 0.01$). Averaged gels were generated for mice with gel replicates, and the number of replicates is indicated in parentheses. Each column is a single protein's expression across each mouse. Green = down regulated, Red = up regulated. (**B**), Identified up regulated and down regulated proteins between day 5 and day 7. The numbers in parentheses correspond to their location in Figure 2.

domains 1/2, 3 contained domains 2/3, and 2 contained domain 3, as detected by MALDI MS. There exist hydrophobic sites in the linker regions of albumin; however we can only propose that cathepsin D is interacting with albumin in this system and acting at these sites. Regardless, we see an increase in cathepsin D during tumor progression (Figure 5B) supporting other reports that show cathepsin D expression is a good prognostic indicator for negative outcomes in some cancers.[26,27] Interestingly, B16-F10 cells in medium containing 10% fetal bovine serum, a rich source of albumin, express levels of cathepsin D similar to the highly vascularized day 7 and day 10 tumors (Figure 5B).

Table 2. Albumin Species[a,b]

spot no.	span of peptides observed by MALDI-TOF	theoretical M_r ($\times 10^{-3}$)[c]	estimated M_r ($\times 10^{-3}$)[d]
10	243−602	40	49
22	35−604	65	72
26	45−452	46	52
27	35−372	39	41
28	25−434	47	41
29	265−602	38	45
30	45−569	59	60
31	45−602	63	49
32	422−602	20	28
33	361−602	27	28
34	35−524	55	44
35	25−168	16	22
44	25−372	40	43
48	35−604	65	72
49	45−602	63	65
50	234−602	41	49
51	35−434	45	51
52	89−452	41	53
53	461−602	16	18
58	348−524	20	31

[a] Spot numbers correspond with the gel image in Figure 2. [b] Albumin is synthesized in the liver as a 608 aa preproprotein, containing a signal sequence at residues 1−18, a propeptide from residues 19−24, and secreted albumin from 25 to 608. [c] Estimated relative molecular weights based on the span of peptides observed by MALDI-TOF mass spectrometry. [d] Estimated relative molecular weights based on gel migration.

These rapidly growing tumors were also undergoing angiogenesis as seen with the rich network of vessels feeding into the tumor mass (Figure 1A). Angiogenesis is a crucial process in the maintenance of tumor growth by providing a network for nutrients and oxygen to reach tumor cells.[28] Hemoglobins alpha and beta are oxygen transporters in the blood, and their increase during early tumor progression (Table 1) reflects the increased vascularization in the tumor microenvironment. The angiogenic switch is an early event in tumorigenesis characterized by the secretion of pro-angiogenic factors such as VEGFs and angiopoietins.[19] In the B16-F10 tumor model of melanoma, the angiogenic switch may be initiated earlier than day 3 with other angiogenic factors being expressed, but we do not detect VEGF expression until day 5 within these tumors (Figure 5B). The CD31 staining correlates with VEGF expression because we do not see blood vessels within the tumor until after day 3 (Figure 5A). Interestingly, one of the VEGF isoforms increases between day 3 and day 7, and then decreases between day 7 and day 10 indicating a potential regulatory mechanism for VEGF expression. It is not surprising that we found epidermal fatty acid binding protein 5 (Figure 4B, Trend 5) following a similar trend as this isoform of VEGF. The increase in epidermal fatty acid binding protein between day 3 and day 7, may represent a wounding response,[29] and the processes of angiogenesis and wounding have been reported to be very similar.[30] We would expect VEGF and epidermal fatty acid binding protein 5 expression to increase from day 7 to day 10 in response to angiogenesis. However, our trend analysis revealed that protein expression was not just continuously increasing or decreasing, and this demonstrated the dynamic processes occurring during tumor progression.

The B16-F10 tumors also demonstrated protein expression and histological characteristics of a hypoxic or reduced tissue oxygen tension, tumor mass (Table 1, Figures 1C and 5).

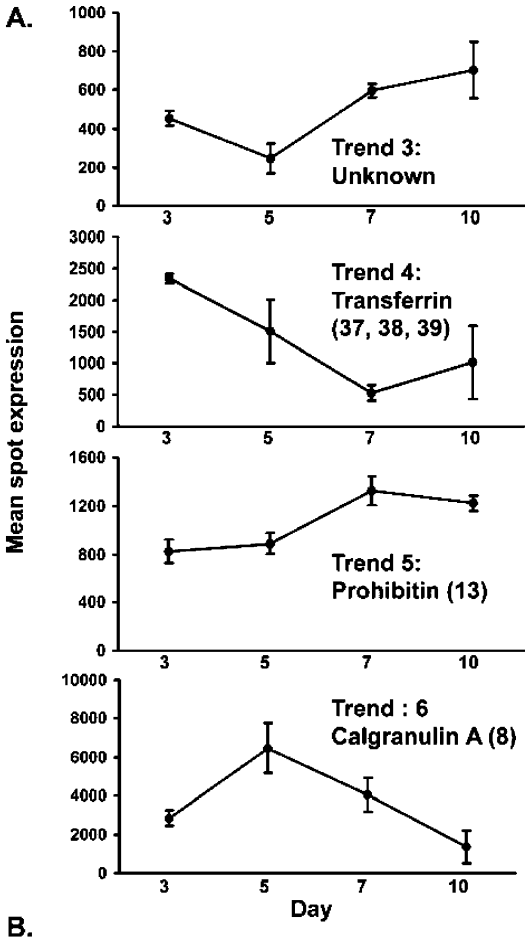

B.

Trend 1: Continuous increase in spot expression
Chaperonin subunit 2 (beta) (61)
Hemoglobin beta (6)
Hemoglobin alpha (7)
Gamma-actin (43)
3-phosphoglycerate dehydrogenase (59)

Trend 2: Continuous decrease in spot expression
Albumin 1 (22, 27, 28, 29, 32, 33, 44, 49, 51, 52)
Peroxiredoxin 5 (60)

Trend 4:
Enolase 1, alpha non-neuron (36)

Trend 5:
Adenylate kinase 2 (11)
Fatty acid binding protein 5, epidermal (18)
Pyrophosphatase (20)

Trend 6:
Albumin 1 (26, 53)
Chloride intracellular channel 1 / Serum albumin - mouse (fragment) (58)

Figure 4. (**A**) Four protein's trends identified by the Jonckheere-Terpstra (J−T) test. The J−T test evaluated ordered differences among the groups (days 3, 5, 7, and 10), and 12 different orderings were tested. The J−T test found 53 protein spots with significant trends ($p < 0.001$). Six predominant trends were identified. Trend 1 increased continuously, and Trend 2 decreased continuously. An unknown protein, transferrin, prohibitin, and calgranulin A are shown and represent Trends 3−6. Error bars represent the standard deviation of the individual spot expression for the mice in each group. If a spot was not present in 2 or more of the groups it was omitted from the test. The numbers in parentheses correspond to their location in Figure 2. (**B**) Identified proteins fitting a particular trend. The numbers in parentheses correspond to their location in Figure 2.

Another major function of albumin is the maintenance of capillary and tissue oncotic pressure. Albumin accounts for 65−70% of the capillary plasma oncotic pressure.[31] Tumor capillaries are considered leaky,[32] and when capillary barriers are more permeable to proteins such as albumin, tissue oncotic pressure increases. Interstitial tumor pressure has been reported as high as 20−50 mmHg compared to normal tissue, 0−0.4 mmHg.[33] Elevated intratumoral oncotic pressure ultimately results in blood stasis in the tumor tissue vessels.[24] Without proper filtering of the blood, and a supply of nutrients to the tumor cells, areas of the tumor become hypoxic and necrotic. Evidence of this event in the B16-F10 tumor can be seen as early as day 5, but more prominent in the day 7 and day 10 tumors (Figure 1C). The degradation of albumin by tumors could also be a mechanism by which tumors reduce interstitial pressure to help promote circulation. Hypoxia has been reported to be a major regulator in tumor progression,[34] and a lack of oxygen often promotes a more aggressive tumor.[35] Evidence of necrosis in these tumors is also supported by the recruitment and invasion of macrophages to the tumor (Figure 5A). Recruitment of inflammatory cells (mast cells) to tissues, and the soluble factors they release, promotes the angiogenic switch that has been described by Coussens et al.[36]

Other proteins that were up regulated between day 3 and day 5 are involved in protein folding and biosynthesis, calcium binding, cell cycle regulation, RNA processing, and chemotaxis. Calgranulin A and B, members of the S100 family of proteins, were increased which has been shown to be a serum marker for metastatic melanoma in humans;[37] therefore, it is plausible that other family members of these proteins are increased in serum levels in tumor bearing mice. This group of proteins also contains the translationally controlled tumor protein (TCTP) which has been shown to be involved in cell cycle regulation, calcium binding, and triggers histamine release in basophils.[38] B16-F10 cell line expression of TCTP protein parallels expression in the day 5 tumor, and the protein expression remains unchanged at day 7 (data not shown). The drop in TCTP expression from cell culture to day 3, and then recovery at day 5, may indicate that the cells were initially stressed from the injection process and needed time to adapt to their new environment.

Proteins down regulated from day 3 to day 5 are associated with electron transport, protein folding, blood coagulation, and transport. Transferrin is within this group, and in Trend 4 (Figure 4A) Transferrin was also present as a train of spots (Figure 2, spots 37−40), representing charged isoforms of the protein. Transferrin is synthesized in the liver, transports Fe in the serum and delivers it to cells through transferrin receptor 1 (TfR1).[39] Some cancer cells have been shown to have higher levels of TfR1,[40] and consume Fe at a higher rate.[41] The transferrin molecule has a half-life of 8 days and may be used up to 100 times for iron delivery.[42] It is unclear if the decrease in transferrin is a result rapid turn over of the protein because of high Fe consumption by the tumor.

Prohibitin, superoxide dismutase, and alpha enolase are regulated proteins between day 5 and day 7 that have been described as mediators in cancer biology. Prohibitin was increased 1.5-fold, and has recently been described as positive regulator of melanogenesis.[43] Superoxide dismutase, an antioxidant protein that has been implicated in promoting tumor growth, was increased 1.4-fold.[44] One form of alpha enolase (Figure 2, spot 36) was down regulated 1.7-fold, and down regulation of alpha enolase has been shown to be a good

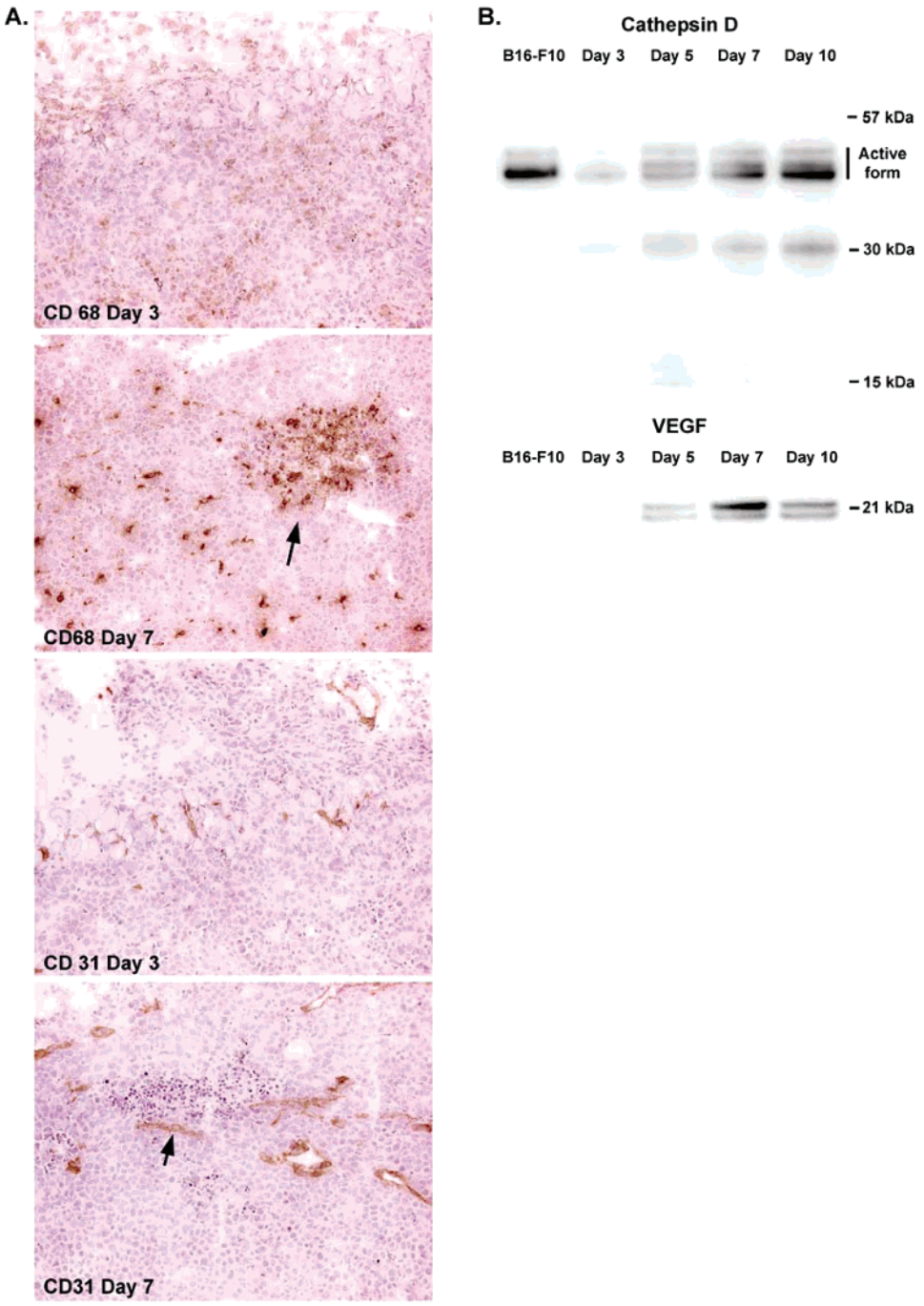

Figure 5. (**A**) Macrophage (CD68) and Endothelial cell (CD31) staining on day 3 and day 7 tumors (20× lens magnification). Black arrows indicate areas of necrosis in the tumor mass. (**B**) Immunoblotting of 1D gels probing cathepsin D (4 μg load) and VEGF (8 μg load) in B16-F10 cell lysates and days 3, 5, 7, and 10 tumors. Cathepsin D is synthesized as a prepro-enzyme and after proteolytic cleavages produces the active form of the protein (42 kDa). The protein undergoes further proteolytic cleavage into heavy (30 kDa) and a light (13 kDa) chains under denaturing conditions. Two bands were detected with the VEGF antibody.

prognostic factor for aggressive tumors in nonsmall cell lung cancer patients.[45] Down regulation of this protein may correspond with down regulation of myc binding protein-1 (MBP-1). MBP-1 is a negative regulator of the c-myc protooncogene and overexpression of c-myc has been described in many malignant cell types.[46,47]

2D gel electrophoresis has been plagued by random technical variations in all aspects of the technique, such as protein staining, image collection, and variable representation of proteins on gels.[48] To help minimize variation associated with 2D gels, software packages such as the ones used in this study are available to determine statistically significant changes in protein expression among sample replicates. Regardless of the approach for selecting interesting spots to further characterize by mass spectrometry, it is still a challenge to identify those proteins of biological interest that are truly differentially expressed between different physiological conditions, while minimizing false positives and false negatives. Multiple statistical approaches gave us high confidence in the proteins that were selected as being differentially expressed in the tumor

mass. This was supported by the considerable overlap in the proteins identified in each statistical analysis. For example, 37 of the 44 (84%) proteins identified in the switch between day 5 and day 7 were also identified as being significant in either the tumor kinetic classifications and/or in the trend analysis.

The goal of this study was to elucidate the processes of tumor progression by identifying differentially expressed proteins within the tumor mass so that these proteins could be used as novel therapeutic targets to be knocked down or overexpressed in the B16-F10 tumor cell line, or in the case of stroma cells, ECM components or soluble factors in the tumor microenvironment, targeted with small molecules. Using large format gels, it is possible to obtain a profile of the relative concentrations of up to 2000 of the proteins expressed in cells or in a tissue. However, it is estimated that the number of expressed proteins in mammalian cells or tissues is on the order of magnitude of 10^6, far exceeding the dynamic range of 2D gels. High concentration proteins are often a large portion of the protein resolved on a 2D gel.[49] In our study, high concentration proteins have demonstrated processes associated with tumor progression, and what will prove interesting is correlating these data with future studies on low concentration proteins.

Acknowledgment. This work was supported in part by the Intramural Research Program of the NIH, National Eye Institute. This work was also supported partly by grants from the Cancer Society in Stockholm, the Swedish Cancer Society, the EU 6-FP "ALLOSTEM" (LSHB-CT-2004-502219) and U.S. Department of Defense Prostate Cancer Research Program (PC030958).We thank Kynita Winn for SDS-PAGE technical assistance, Ewa Jankowska-Stephens for mass spectrometry technical assistance, and George Reed for help with the statistical analyses. We also thank Gustav Wallmark, Andreas Olsson, and Ola Forsstrom-Olsson of Ludesi for helpful discussions on the data and statistical analysis.

References

(1) Ortega, A.; Ferrer, P.; Carretero, J.; Obrador, E.; Asensi, M. et al. Down-regulation of glutathione and Bcl-2 synthesis in mouse B16 melanoma cells avoids their survival during interaction with the vascular endothelium. *J. Biol. Chem.* **2003**, *278*, 39591−39599.

(2) Melnikova, V. O.; Bolshakov, S. V.; Walker, C.; Ananthaswamy, H. N. Genomic alterations in spontaneous and carcinogen-induced murine melanoma cell lines. *Oncogene* **2004**, *23*, 2347−2356.

(3) Agrawal, S.; Reemtsma, K.; Bagiella, E.; Oluwole, S. F.; Braunstein, N. S. Role of TAP-1 and/or TAP-2 antigen presentation defects in tumorigenicity of mouse melanoma. *Cell. Immunol.* **2004**, *228*, 130−137.

(4) Blank, C.; Brown, I.; Kacha, A. K.; Markiewicz, M. A.; Gajewski, T. F. ICAM-1 contributes to but is not essential for tumor antigen cross-priming and CD8+ T cell-mediated tumor rejection in vivo. *J. Immunol.* **2005**, *174*, 3416−3420.

(5) Kashiwagi, S.; Izumi, Y.; Gohongi, T.; Demou, Z. N.; Xu, L. et al. NO mediates mural cell recruitment and vessel morphogenesis in murine melanomas and tissue-engineered blood vessels. *J. Clin. Invest.* **2005**, *115*, 1816−1827.

(6) Kakuta, S.; Tagawa, Y.; Shibata, S.; Nanno, M.; Iwakura, Y. Inhibition of B16 melanoma experimental metastasis by interferon-gamma through direct inhibition of cell proliferation and activation of antitumor host mechanisms. *Immunology* **2002**, *105*, 92−100.

(7) D'Agostini, C.; Pica, F.; Febbraro, G.; Grelli, S.; Chiavaroli, C. et al. Antitumor effect of OM-174 and cyclophosphamide on murine B16 melanoma in different experimental conditions. *Int. Immunopharmacol.* **2005**, *5*, 1205−1212.

(8) Dranoff, G.; Jaffee, E.; Lazenby, A.; Golumbek, P.; Levitsky, H. et al. Vaccination with irradiated tumor cells engineered to secrete murine granulocyte-macrophage colony-stimulating factor stimulates potent, specific, and long-lasting antitumor immunity. *Proc. Natl. Acad. Sci. U.S.A.* **1993**, *90*, 3539−3543.

(9) van Elsas, A.; Hurwitz, A. A.; Allison, J. P. Combination immunotherapy of B16 melanoma using anti-cytotoxic T lymphocyte-associated antigen 4 (CTLA-4) and granulocyte/macrophage colony-stimulating factor (GM-CSF)-producing vaccines induces rejection of subcutaneous and metastatic tumors accompanied by autoimmune depigmentation. *J. Exp. Med.* **1999**, *190*, 355−366.

(10) Kurisu, S.; Suetsugu, S.; Yamazaki, D.; Yamaguchi, H.; Takenawa, T. Rac-WAVE2 signaling is involved in the invasive and metastatic phenotypes of murine melanoma cells. *Oncogene* **2005**, *24*, 1309−1319.

(11) van Kempen, L. C.; Ruiter, D. J.; van Muijen, G. N.; Coussens, L. M. The tumor microenvironment: a critical determinant of neoplastic evolution. *Eur. J. Cell Biol.* **2003**, *82*, 539−548.

(12) Li, G.; Satyamoorthy, K.; Meier, F.; Berking, C.; Bogenrieder, T. et al. Function and regulation of melanoma-stromal fibroblast interactions: when seeds meet soil. *Oncogene* **2003**, *22*, 3162−3171.

(13) Liotta, L. A.; Kohn, E. C. The microenvironment of the tumor-host interface. *Nature* **2001**, *411*, 375−379.

(14) Jonckheere, A. A distribution-free K sample test against ordered alternatives. *Biometrika* **1954**, *41*, 133−145.

(15) Anderson, L. *Two-Dimensional Electrophoresis: Operation of the ISO-DALT* System; second Ed. ed.; Large Scale Biology Press: Rockville, MD, 1991; 128−130.

(16) da Silva, R. P.; Gordon, S. Phagocytosis stimulates alternative glycosylation of macrosialin (mouse CD68), a macrophage-specific endosomal protein. *Biochem. J.* **1999**, *338* (Pt 3), 687−694.

(17) Papetti, M.; Herman, I. M. Mechanisms of normal and tumor-derived angiogenesis. *Am. J. Physiol. Cell Physiol.* **2002**, *282*, C947−970.

(18) Vecchi, A.; Garlanda, C.; Lampugnani, M. G.; Resnati, M.; Matteucci, C. et al. Monoclonal antibodies specific for endothelial cells of mouse blood vessels. Their application in the identification of adult and embryonic endothelium. *Eur. J. Cell Biol.* **1994**, *63*, 247−254.

(19) Ruoslahti, E. Specialization of tumor vasculature. *Nat. Rev. Cancer* **2002**, *2*, 83−90.

(20) Mego, J. L. Role of thiols, pH and cathepsin D in the lysosomal catabolism of serum albumin. *Biochem. J.* **1984**, *218*, 775−783.

(21) Compaine, A.; Schein, J. D.; Tabb, J. S.; Mohan, P. S.; Nixon, R. A. Limited proteolytic processing of the mature form of cathepsin D in human and mouse brain: postmortem stability of enzyme structure and activity. *Neurochem. Int.* **1995**, *27*, 385−396.

(22) Baynes, J. W.; Thorpe, S. R. Identification of the sites of albumin catabolism in the rat. *Arch. Biochem. Biophys.* **1981**, *206*, 372−379.

(23) Andersson, C.; Iresjo, B. M.; Lundholm, K. Identification of tissue sites for increased albumin degradation in sarcoma-bearing mice. *J. Surg. Res.* **1991**, *50*, 156−162.

(24) Stehle, G.; Sinn, H.; Wunder, A.; Schrenk, H. H.; Stewart, J. C. et al. Plasma protein (albumin) catabolism by the tumor itself—implications for tumor metabolism and the genesis of cachexia. *Crit. Rev. Oncol. Hematol.* **1997**, *26*, 77−100.

(25) Offermann, M. K.; Chlebowski, J. F.; Bond, J. S. Action of cathepsin D on fructose-1,6-bisphosphate aldolase. *Biochem. J.* **1983**, *211*, 529−534.

(26) Zeillinger, R.; Swoboda, H.; Machacek, E.; Nekahm, D.; Sliutz, G. et al. Expression of cathepsin D in head and neck cancer. *Eur. J. Cancer* **1992**, *28A*, 1413−1415.

(27) Johnson, M. D.; Torri, J. A.; Lippman, M. E.; Dickson, R. B. The role of cathepsin D in the invasiveness of human breast cancer cells. *Cancer Res.* **1993**, *53*, 873−877.

(28) Folkman, J. What is the evidence that tumors are angiogenesis dependent? *J. Natl. Cancer Inst.* **1990**, *82*, 4−6.

(29) Schurer, N. Y. Implementation of fatty acid carriers to skin irritation and the epidermal barrier. *Contact Dermatitis* **2002**, *47*, 199−205.

(30) Robinson, S. C.; Coussens, L. M. Soluble mediators of inflammation during tumor development. *Adv. Cancer Res.* **2005**, *93*, 159−187.

(31) Mehta, D.; Malik, A. B. Signaling mechanisms regulating endothelial permeability. *Physiol. Rev.* **2006**, *86*, 279−367.

(32) Carmeliet, P. VEGF as a key mediator of angiogenesis in cancer. *Oncology* **2005**, *69 Suppl 3*, 4−10.

(33) Boucher, Y.; Jain, R. K. Microvascular pressure is the principal driving force for interstitial hypertension in solid tumors: implications for vascular collapse. *Cancer Res.* **1992**, *52*, 5110−5114.
(34) Harris, A. L. Hypoxia—a key regulatory factor in tumor growth. *Nat. Rev. Cancer* **2002**, *2*, 38−47.
(35) Bottaro, D. P.; Liotta, L. A. Cancer: Out of air is not out of action. *Nature* **2003**, *423*, 593−595.
(36) Coussens, L. M.; Raymond, W. W.; Bergers, G.; Laig-Webster, M.; Behrendtsen, O. et al. Inflammatory mast cells up-regulate angiogenesis during squamous epithelial carcinogenesis. *Genes Dev.* **1999**, *13*, 1382−1397.
(37) Bottoni, U.; Izzo, P.; Richetta, A.; Mannooranparampil, T. J.; Devirgiliis, V. et al. S100 serum level: a tumor marker for metastatic melanoma. *Melanoma Res.* **2003**, *13*, 427−429.
(38) Bommer, U. A.; Thiele, B. J. The translationally controlled tumor protein (TCTP). *Int. J. Biochem. Cell Biol.* **2004**, *36*, 379−385.
(39) Kwok, J. C.; Richardson, D. R. The iron metabolism of neoplastic cells: alterations that facilitate proliferation? *Crit. Rev. Oncol. Hematol.* **2002**, *42*, 65−78.
(40) Larrick, J. W.; Cresswell, P. Modulation of cell surface iron transferrin receptors by cellular density and state of activation. *J. Supramol. Struct.* **1979**, *11*, 579−586.
(41) Richardson, D.; Baker, E. Two mechanisms of iron uptake from transferrin by melanoma cells. The effect of desferrioxamine and ferric ammonium citrate. *J. Biol. Chem.* **1992**, *267*, 13972−13979.
(42) Harford, J. B., Rouault, T. A., Huebers, H. A., Klausner, R. D. Molecular mechanisms of iron metabolism. *In The Molecular* Basis of Blood Diseases; W. B. Saunders Co.: Philadelphia, PA, 1994; 351−378.
(43) Snyder, J. R.; Hall, A.; Ni−Komatsu, L.; Khersonsky, S. M.; Chang, Y. T. et al. Dissection of melanogenesis with small molecules identifies prohibitin as a regulator. *Chem. Biol.* **2005**, *12*, 477−484.
(44) Schiff, R.; Reddy, P.; Ahotupa, M.; Coronado-Heinsohn, E.; Grim, M. et al. Oxidative stress and AP-1 activity in tamoxifen-resistant breast tumors in vivo. *J. Natl. Cancer Inst.* **2000**, *92*, 1926−1934.
(45) Chang, Y. S.; Wu, W.; Walsh, G.; Hong, W. K.; Mao, L. Enolase-alpha is frequently down-regulated in nonsmall cell lung cancer and predicts aggressive biological behavior. *Clin. Cancer Res.* **2003**, *9*, 3641−3644.
(46) Jenkins, R. B.; Qian, J.; Lieber, M. M.; Bostwick, D. G. Detection of c-myc oncogene amplification and chromosomal anomalies in metastatic prostatic carcinoma by fluorescence in situ hybridization. *Cancer Res.* **1997**, *57*, 524−531.
(47) Smith, D. R.; Myint, T.; Goh, H. S. Overexpression of the c-myc proto-oncogene in colorectal carcinoma. *Br. J. Cancer* **1993**, *68*, 407−413.
(48) Dowsey, A. W.; Dunn, M. J.; Yang, G. Z. The role of bioinformatics in two-dimensional gel electrophoresis. *Proteomics* **2003**, *3*, 1567−1596.
(49) Gygi, S. P.; Corthals, G. L.; Zhang, Y.; Rochon, Y.; Aebersold, R. Evaluation of two-dimensional gel electrophoresis-based proteome analysis technology. *Proc. Natl. Acad. Sci. U.S.A.* **2000**, *97*, 9390−9395.

PR060059Q